Unraveling the Structure and Role of Mn and Ce for Selective Catalytic Reduction of NOx in Application-Relevant Catalysts and Conditions

Lieven Gevers
  King Abdullah University of Science and Technology

Linga Enakonda
  KAUST

Ameen Shahid
  KAUST

Samy Ould-Chikh
  King Abdullah University of Science and Technology (KAUST)   https://orcid.org/0000-0002-3486-0944

Pasi Paalanen
  KAUST

Mohamed Hedhili
  KAUST

Fei Wen
  Umicore AG & Co

Javier Ruiz-Martinez (✉ javier.ruizmartinez@kaust.edu.sa)
  KAUST   https://orcid.org/0000-0002-9850-7939

Article

---

1   **Unraveling the Structure and Role of Mn and Ce for Selective Catalytic**

2   **Reduction of NOx in Application-Relevant Catalysts and Conditions**

3

4   **Lieven E. Gevers[1], Linga R. Enakonda[1], Ameen Shahid[1], Samy Ould-Chikh[1], Pasi P. Paalanen[1],**

5   **Mohamed Nejib Hedhili[2], Fei Wen[3] and Javier Ruiz-Martínez[1*]**

6

7   [1] King Abdullah University of Science and Technology, KAUST Catalysis Center, Thuwal 23955, Saudi

8   Arabia

9   [2] King Abdullah University of Science and Technology, KAUST Core Labs, Thuwal 23955, Saudi Arabia

10   [3]Umicore AG & Co. KG, Rodenbachen Chaussee 4, 63457 Hanau-Wolfgang, Germany.

11   [*]e-mail: Javier.ruizmartinez@kaust.edu.sa

12

13

Abstract

Mn-based oxides are promising catalysts for the selective catalytic reduction (SCR) of NOx with NH_3 at temperatures below 200 ˚C. There is a general agreement that combining Mn with another metal oxide, such as CeOx improves catalytic activity. However, to date, there is an unsettling debate on the role of Ce as Mn promoter on the SCR reaction. To solve this, here we have systematically studied the effect Ce by preparing, characterizing and testing around 30 catalysts aiming for a well-controlled homogeneous dispersion of the metal oxides. Our results show that, at low-temperature SCR conditions, the intrinsic activity of the Mn active sites is not positively affected by Ce species in intimate contact. In fact, the results suggest that Ce is electronically interacting with Mn and decreasing the active-site average activity. To confirm our findings, activities reported in literature were surface-area normalized and the analysis do not support an increase in activity by Ce addition. Therefore, we can unequivocally conclude that the beneficial effect of Ce is textural, increasing catalyst surface area and therefore the total number of active sites. Besides, addition of Ce is increasing N_2 selectivity as it suppresses second-step oxidation reactions and thus N_2O formation by structurally diluting the MnOx active sites. Therefore, the textural promoting effect still makes Ce an interesting additive for Mn catalysts.

30

Introduction

The selective catalytic reduction (SCR) of environmentally harmful nitric oxide (NO) with ammonia (NH$_3$) is a well-known and established technology for the denitrification of exhaust gases from stationary (power plant) and mobile (e.g. lean burn engines) sources.[1-3] However, the more stringent global legislations and the relatively low exhaust temperatures of more efficient engines and low-load engine operations require the search for more efficient catalytic systems. For example, In Euro 6 stage the European Union legislative authorities have tightened the limits of nitrogen oxides being emitted from diesel cars (from 180 mg NO$_x$/km in Euro 5 to 80 mg NO$_x$/km in Euro 6).[4] A wide variety of catalytic systems based on metal-containing zeolites and mixed metal oxides have been investigated in this reaction. The introduction of Cu-exchanged small pore molecular sieves such as Cu-SSZ-13 and Cu-SAPO-34 have been a revolutionary technology for SCR applications[5] and have an optimal performance between 200 – 450 °C.[6-8] Among mixed metal oxides, V$_2$O$_5$-WO$_3$-/TiO$_2$ catalysts give more than 90 % NO conversion at gas hourly space velocities (GHSV) of 60000 – 90000 h^{-1} between 250 – 400 °C.[9-13] However, all these systems fall short of providing sufficient performance at temperatures below 200 °C. Catalyst operating at lower temperatures are imperative in mobile applications due to engine cold start[14] and new advances in low-temperature combustion[15]. In this respect, manganese-containing mixed metal oxides exhibit excellent catalytic activity in the NH$_3$-SCR reaction operating at temperatures below 200 °C, and therefore is of particular interest as a potential low-temperature component in NH$_3$-SCR.[16-20]

Typically, Mn-based catalysts are prepared by impregnation or homogeneous precipitation methods with other metal oxides, such as Ti and Ce oxides, that act as support, dopants or promoters. During the last decades, the role of the different components on the catalytic activity and selectivity have been debated extensively[3]. Mn catalytic activity originates from its excellent redox ability at low temperatures. The importance of specific surface area, dispersion and oxidation state of the different Mn oxides have been highlighted[21-23]. TiO$_2$ is considered a metal oxide support providing optimal dispersion of Mn active species, surface area, thermal stability and Lewis acid sites to adsorb NH$_3$[24, 25].

57   For Ce and other transition metal, there is no clear consensus on their role on the catalytic reaction.

58   The promotional effect is often explained by an improvement of the catalytic redox cycles by intimate

59   contact of the active Mn oxides and the promotors[26-28]. Among the transition metals, Ce is widely used

60   and probably one of the most promising promotors[3]. In binary MnCe systems, the addition of Ce was

61   reported to improve the conversion levels compared to individual Mn oxides[29, 30]. This promotional

62   effect is generally explained by an enhancement of the redox functionality, which is proven by the

63   easier reduction of Ce and/or Mn during temperature-programmed reduction experiments[31]. Baiker

64   et al. also postulated that binary MnCe oxides have a higher adsorption of NO and NH_3, which

65   promotes catalytic activity[32]. In ternary MnCeTi oxides, the improvement of activity by Ce is also

66   frequently explained by an increase of the Mn redox properties[31, 33-35]. In contrast, other studies

67   suggest that the Mn-Ce electronic interaction decrease the activity of Mn species for NO conversion[36]

68   by a reduction of the Mn^{4+}/Mn^{3+} ratio. On the basis of the measured surface areas, binary MnCe[29, 30,

69   32] and tertiary MnCeTi[31, 33, 36-38] systems show better textural properties when Ce is added, but this is

70   rarely discussed as a main promoting effect.

71   To resolve this unsettled dilemma, we studied the structure and catalytic performance of Mn, Ce and

72   Ti mixed-oxide catalysts with a wide range of metal-oxide compositions. The catalysts were prepared

73   by a homogeneous precipitation method designed to obtain mixed oxides with amorphous structure

74   and a homogeneous dispersion of the distinct metal oxides. More specifically, 30 catalysts were

75   systematically synthesized with different Mn, Ce and Ti compositions. To verify the formation of an

76   amorphous and homogeneous mixed oxide, we have chosen a multi-technique approach combining

77   XRD, electron microscopy and high-resolution X-ray photoelectron spectroscopy. The low

78   temperature NH_3-SCR performance of all the catalysts was investigated under relevant conditions

79   encountered in a car exhaust.

80

81

82   **Catalyst synthesis, structure and metal-oxide spatial distribution.**

83   After synthesis of the catalysts, we aim to characterize their structure and chemical properties by a

84   multi-pronged approach. The crystalline structure of the catalysts was studied by powder X-ray

85   diffraction, and crystallite sizes were calculated from diffraction peaks integral breadth using the

86   Scherrer equation. The results are summarized in the ternary diagram plotted in Fig. 1 and the detailed

87   diffraction patterns and crystallite size analysis are in the Supplementary information (Supplementary

88   Fig. 2, Supplementary Fig. 3 and Supplementary Table 2).

89
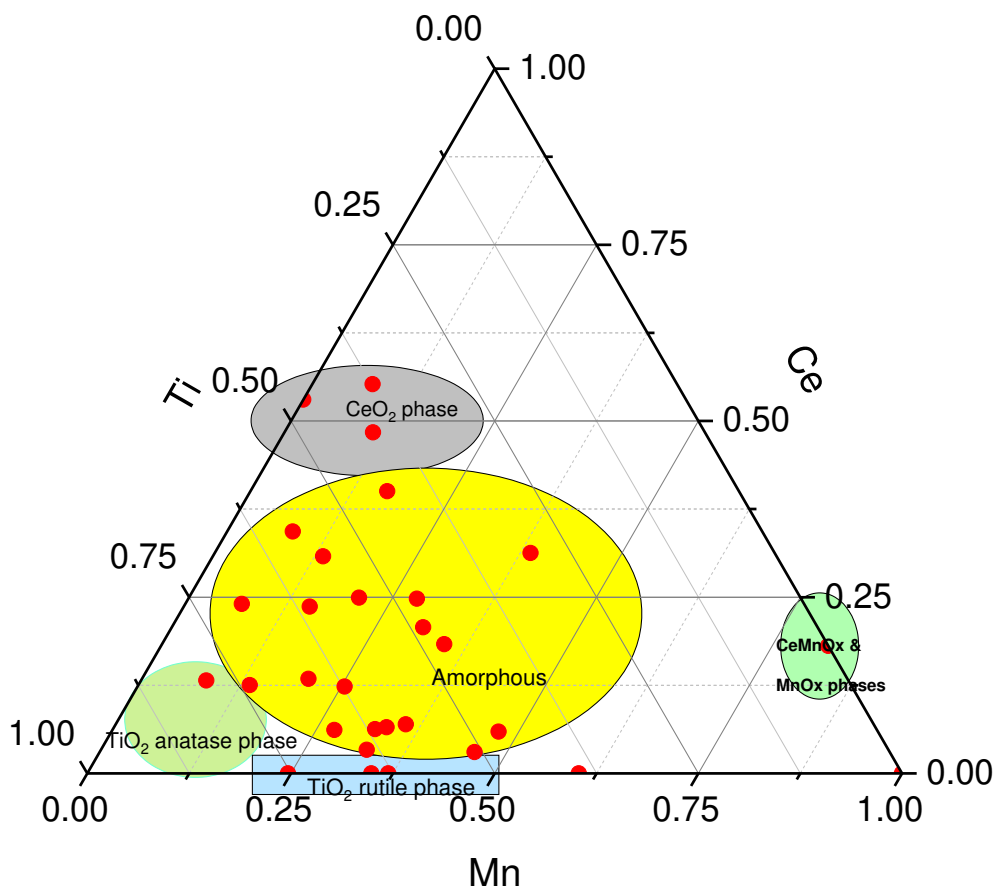
90

91   **Fig. 1.** Ternary phase diagram of the synthesized MnCeTiOx catalyst samples. The colored areas highlight
92   groups of samples with similar crystal phases, measured by XRD.

93

94   The binary catalysts have a certain degree of crystallinity and show reflection lines of fluorite CeO_2

95   structure in the CeTi and MnCe oxides and rutile TiO_2 in the MnTi oxides. MnO_x crystalline phases, α-

96 Mn_2O_3 (Bixbyite), Mn_5O_8, Mn_3O_4 (Hausmannite) and $MnO(OH)$ (Groutite) are observed on the MnCe

97 oxides, whereas binary MnTi samples display weak and broad reflections from MnOx phases,

98 indicating nano-crystallites below 3-4 nm, most likely on the TiO_2 surface. The existence of mono-

99 component metal oxide crystalline phases is an indisputable proof that the preparation method is not

100 successful for the synthesis of well-mixed oxides in binary systems. In sheer contrast to the binary

101 systems, the diffraction patterns of most of the ternary systems show featureless diffraction patterns

102 indicating the amorphous nature of the samples (Supplementary Fig. 3). Only a few samples with high

103 Ti ($Mn_{0.08}Ce_{0.13}Ti_{0.79}$) or Ce ($Mn_{0.07}Ce_{0.55}Ti_{0.37}$ and $Mn_{0.11}Ce_{0.48}Ti_{0.41}$) content display reflections from

104 anatase TiO_2 or fluorite CeO_2, respectively. This suggest that the third metal component facilitates the

105 formation of a ternary amorphous phase, which is the first step on obtaining a homogeneous mixed

106 oxide. Very importantly, the effect of Ce is crucial in the formation of an amorphous phase, as small

107 amounts of such a component inhibits the formation of crystalline phases, as can be observed in the

108 low edge of the ternary diagram in Fig. 1.

109 The bulk and surface composition of the catalysts were compared by using Inductive Coupled Plasma

110 (ICP) and high-resolution X-ray Photoelectron Spectroscopy (XPS), respectively (Supplementary Table

111 1). The bulk chemical composition of the catalysts is comparable with the theoretical composition,

112 with a slight deviation to lower Mn concentrations, which suggests that not all the Mn is precipitated

113 during synthesis. One plausible explanation is the formation of soluble Mn complexes with ammonium

114 ligands, which are less prone to hydrolysis-condensation reactions[39]. Those are expected to remain in

115 the supernatant during the washing by centrifugation, thus decreasing the final Mn content on the

116 catalyst. The bulk composition was compared to the surface composition of selected samples by XPS.

117 For the Mn-Ti binary, there is an enrichment of Mn on the surface, in line with the hypothesis that Mn

118 is supported on TiO_2. For the ternary systems, the results show that surface compositions are similar

119 to bulk compositions, with some of the samples displaying a modest enrichment of Mn and Ce on the

120 surface.

121   To further investigate the structure, metal oxide distribution and local composition of the catalysts,

122   we performed a high-resolution electron microscopy study. A representative transmission electron

123   microscopy (TEM) image of a binary MnTi Sample ($Mn_{0.37}Ce_{0.00}Ti_{0.63}$) is shown in Supplementary Fig. 4.

124   We observed nanosized and crystalline TiO_2 particles decorated with layers of amorphous material.

125   High-angle annular dark-field (HAADF) STEM imaging and elemental mappings computed from energy-

126   dispersive X-ray spectroscopy (EDX) data, presented in Supplementary Fig. 5, reveal that Mn is well

127   dispersed on the TiO_2 particles. In contrast, TEM images of a representative MnCeTi ternary system,

128   in Fig. 2a and b, corroborate the existence of a purely amorphous system. The structural features

129   resemble an agglomeration of shapeless nanoparticles forming a random porous structure. Annular

130   dark-field (ADF) STEM imaging and elemental mapping computed from EELS data confirm the

131   homogeneous distribution of Mn, Ce and Ti metals over individual catalyst particles.
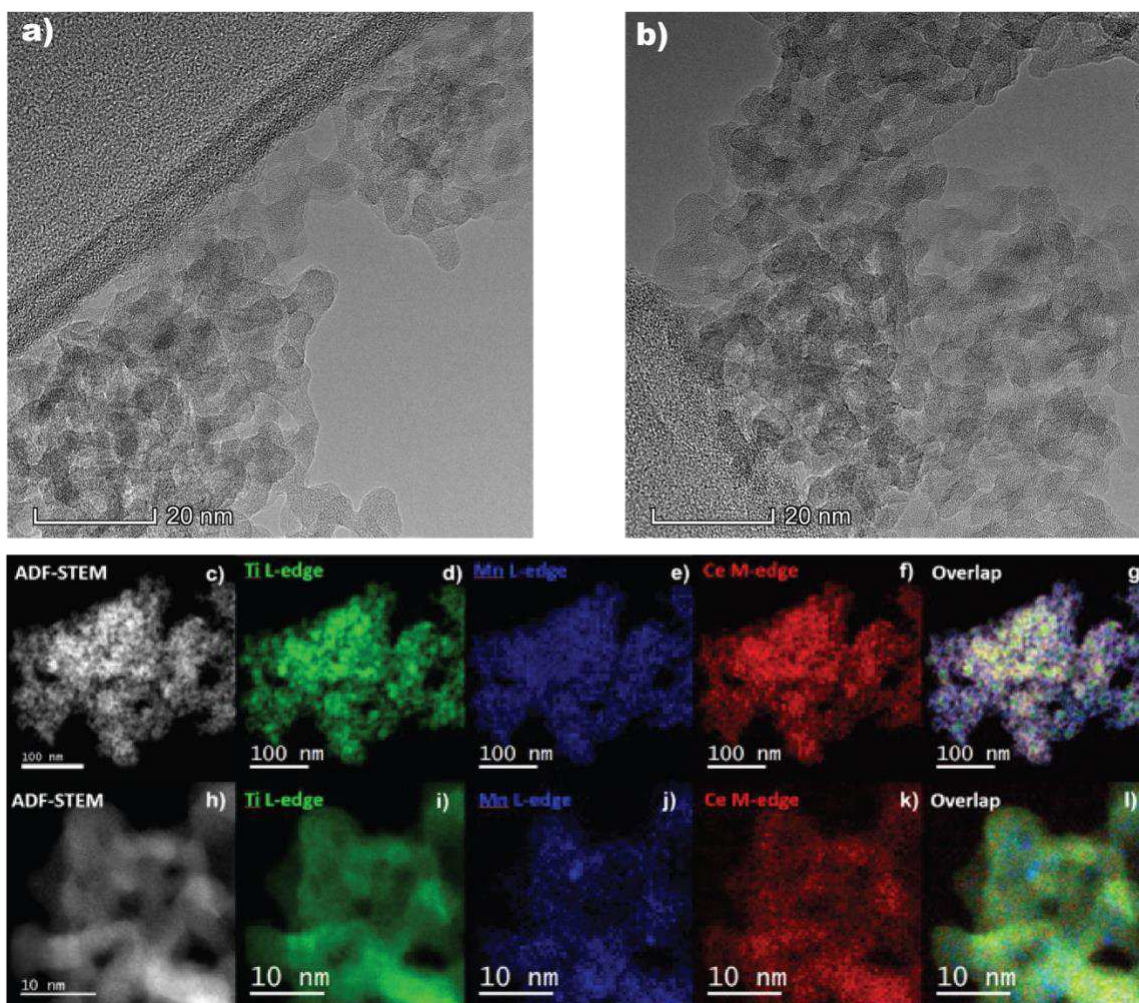
Fig. 2. *(a and b)* Representative HRTEM images of the $Mn_{0.14}Ce_{0.13}Ti_{0.74}$ oxide catalyst. ADF-STEM images and elemental mappings of the same catalyst at (a-d) low and (e-i) high magnification.

All the results strongly confirm that our synthesis route renders a homogeneous distribution of all the metal atoms in the ternary system and indicate that our synthesis method is effective for the preparation of ideal perfectly-mixed ternary metal oxides. From the characterization measurements conducted, we illustrate the structure of the MnTi binary and the MnCeTi ternary catalysts in Fig. 3.

140
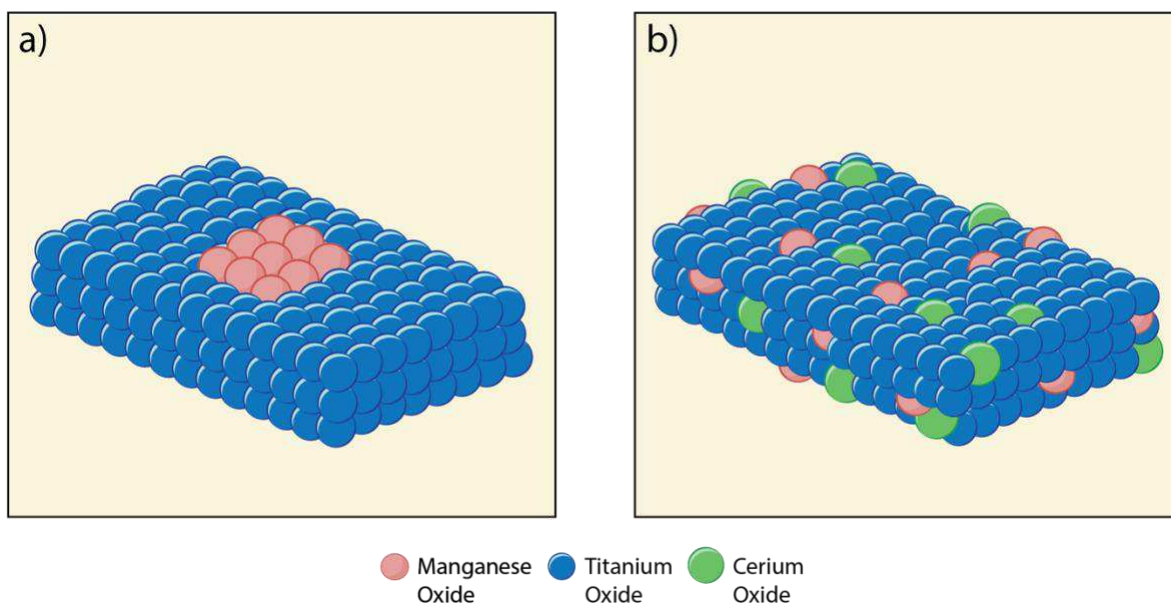
Fig. 3. Schematic representation of a) MnTi binary catalysts where amorphous layers of Mn oxide active are on the surface of crystalline TiO_2 and b) MnCeTi ternary catalysts where the metal oxides are amorphous and well mixed.

Impact of metal oxide composition on catalyst textural properties, oxide reducibility and

speciation. The specific surface areas of the discrete catalysts are presented in the ternary diagram

in Fig. 4 and in supplementary Table 3.

147

148
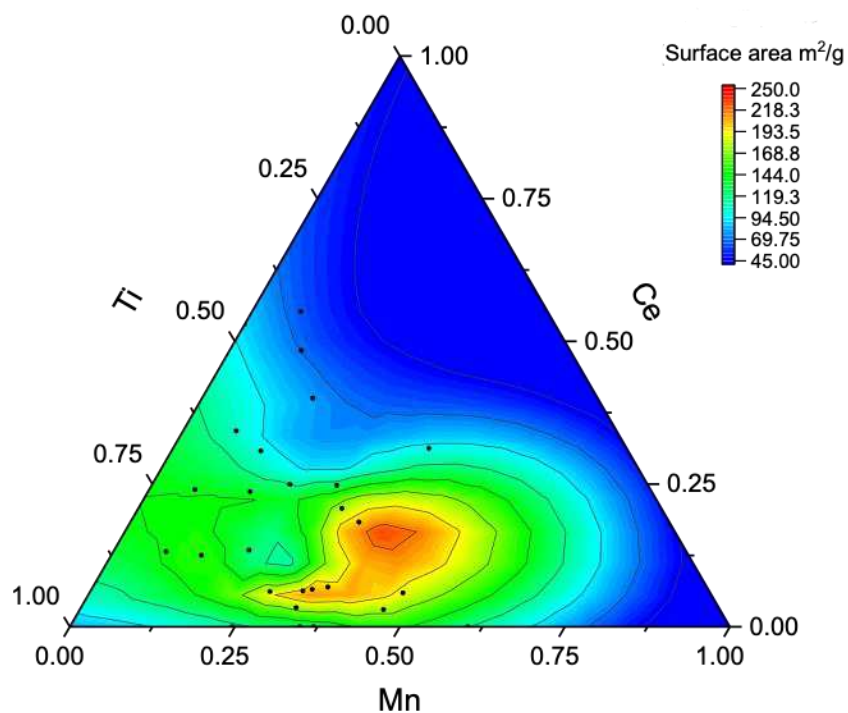
Fig. 4. Ternary diagrams showing the Influence of catalyst composition on BET surface area.

151 The catalyst materials have a clear type IV isotherm, with an H1 loop characteristic of mesoporous

152 coming from the agglomeration of the metal-oxide nanoparticles. Clearly, Ce content has a significant

153 impact on specific surface areas of the ternary catalysts. The addition of Ce plays a key role as

154 structural promotor increasing the surface area from 108 to 245 m^2/g when Ce content increases from

155 0 to 20 mol%. A further increase in Ce has a negative impact and surface areas drop down to 62 m^2/g

156 when Ce concentration reaches 55 mol%, similar to previous studies on Ce-Ti[40], Mn-Ce[41] binary

157 systems and Mn-Ce-Ti ternary systems[42]. Comparing the XRD and BET data, the increase of surface

158 area is strongly correlated with the formation of amorphous structures.

159 To investigate the redox properties of the materials, temperature-programmed reduction (TPR)

160 experiments with H_2 were performed. Overall, the reduction peak at 200-450 °C is attributed to the

161 reduction of Mn^{4+} and Mn^{3+} species to Mn^{2+} [43, 44], whereas the main reduction peak at 550-650 °C is

162 ascribed to the reduction of Ce^{4+} to Ce^{3+} in a mixed oxide phase [45-47]. The difference in the TPR of pure

163 CeO_2, plotted on supplementary Fig. 6, confirms that Ce is well-mixed and strongly interacting with

164 Mn and Ti. The samples containing a low Mn/Ce molar ratio, plotted in Fig. 5a, show a monotonic

165 decrease in the reduction temperature of Ce when Mn content increases. According to literature

166 reports, the main parameters influencing the reduction temperature are specific surface area and the

167 presence of other metals in intimate contact[48]. In this case, the surface area of the binary Ce-Ti system

168 is higher than the Mn-contained samples shown in Fig. 5a. Therefore, changes in the reduction

169 temperature are unrelated to specific surface area and can be rationalized as a consequence of the

170 close proximity of Mn and Ce species, which improves the reducibility and thus the redox properties

171 of Ce. The TPR of samples containing high amount of Mn are shown in Fig. 5b. For the binary Mn-Ti

172 samples, two main peaks from Mn reduction (289-306 °C and 341-408 °C) are observed. Addition of

173 Ce in the catalyst formulation has a strong impact on the TPR profiles: the low temperature peak

174 strongly decreases with small amounts of Ce and the high temperature contribution shifts to higher

175   temperatures with increasing Ce content (see also Supplementary Fig. 7). We surmise that the changes

176   in the TPR profiles probably result from the lower reducibility of the Mn species in close contact with

177   Ce.

178
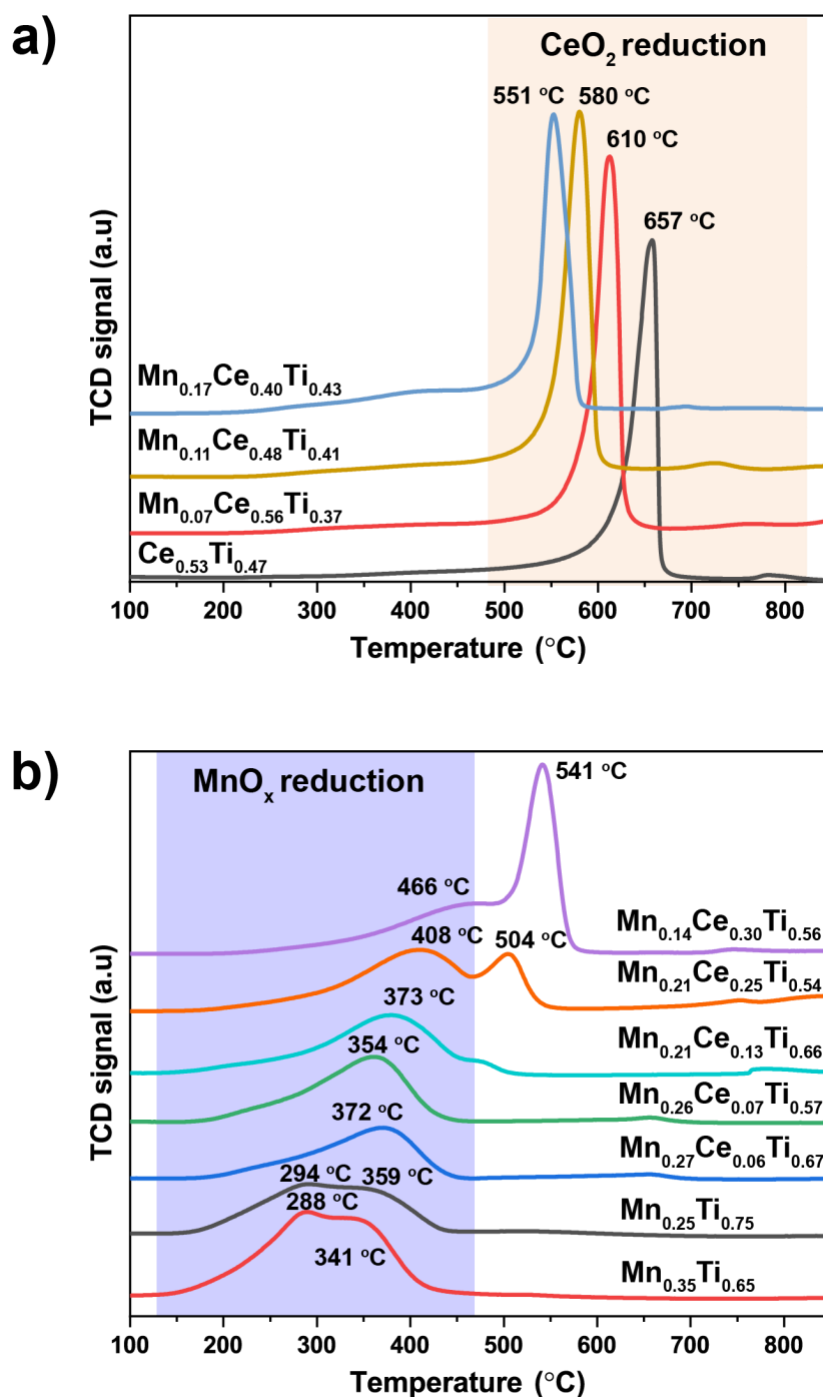
Fig. 5. Temperature-programmed reductions with H_2 of selected samples with a) a low Mn/Ce molar ratio and b) a high Mn/Ce molar ratio. The low-temperature evolution (in purple) is related to the reduction of MnOx phases whereas the high-temperature (in cream) is related to CeO_2 reduction.

182 To gain more nuanced insight into the effect of Ce to the catalyst redox properties, a detailed high-

183 resolution XPS study was performed. Oxidation states of Mn were rigorously fitted from a set of

184 Gaussian-Lorentzian components per oxidation state, due to the multiplet splitting between the

185 unpaired electrons in Mn 2+, 3+ and 4+. The set of components of the discrete oxidation states were

186 obtained from measurements of pure MnO, Mn_2O_3 and MnO_2 oxides and the results were compared

187 with previously reported measurements[49]. More experimental details can be found on the

188 supplementary information and supplementary Fig. 8. The $Mn(2p_{3/2})$ spectra from selected samples

189 show a high amount of Mn^{3+} species in the binary Mn-Ti catalysts, whereas a combination of Mn^{4+} and

190 Mn^{2+} dominates the spectra of ternary samples (see supplementary table 5). There is no clear

191 consensus in the literature on the effect of Ce on the Mn oxidation state. Whilst several authors found

192 an increase in Mn^{3+} species with the addition of $Ce^{31, 35, 36}$, Feng et al. observed a slight reduction in

193 Mn^{3+} [38], and others found no clear correlation[50, 51]. The origin of the discrepancy could be related to

194 the complexity on the analysis of the Mn $(2p_{3/2})$ spectra and the different structure of the prepared

195 catalysts. In order to improve the confidence in our results, average Mn oxidation states were

196 calculated from the XPS and TPR and gave comparable results (see supplementary Table 6), which

197 validates our XPS deconvolution method and confirms that the addition of Ce decreases the average

198 Mn oxidation state. Based on our structural characterization results, we speculate that the reduction

199 in the average Mn oxidation state is due to the existence of Ce species in close proximity to Mn. This

200 might explain the shifting of TPR profile to high temperature after introducing Ce into the MnTi

201 system.

202

203 **Role of Mn and Ce on NO reduction at low temperature.** Next, we inspected the activity of the

204 different samples in the selective catalytic reduction of NO with NH_3 at 150 °C. During the activity

205 measurements, there was no NO_2 formation and the only products were N_2 and N_2O. Activity plot with

206 the amount of Mn shows a close-to-zero intercept of the ordinate, indicating that Mn oxides are the

207 most important species in catalytic performance (Supplementary Fig. 9). Up to 60% of Mn, there is a

208 modest correlation of the increase of activity with the increase in Mn content. However, the results

209 revealed that no evident trend is observed when Mn is above 60% and strongly suggest that Mn

210 content is not the only factor determining catalytic activity.

211 To unravel the effect of the distinct metal oxides, we re-examined the catalytic performance by

212 surface area normalization of the activity. Specific activities (ml of NO converted per m^2 and per min)

213 were plotted as a function of Mn content in Fig. 6. For the individual Mn and the binary Mn-Ti samples,

214 a clear linear dependency of the measured specific activities with the Mn content is observed. The

215 Mn-Ce-Ti ternary systems has also a pseudolinear correlation with the Mn content but with a lower

216 slope. The Mn surface enrichment for the Mn-Ti catalysts observed by XPS (Table S1) can insufficiently

217 explain the almost twofold increase in specific activity. Therefore, we infer that MnO_x species in the

218 individual Mn and binary Mn-Ti catalysts have similar activity, and those are more active than in the

219 Mn-Ce-Ti ternary system. The results are also in line with the higher reduction temperature of

220 manganese species observed in the TPR data of Mn-Ce-Ti ternary systems.

221
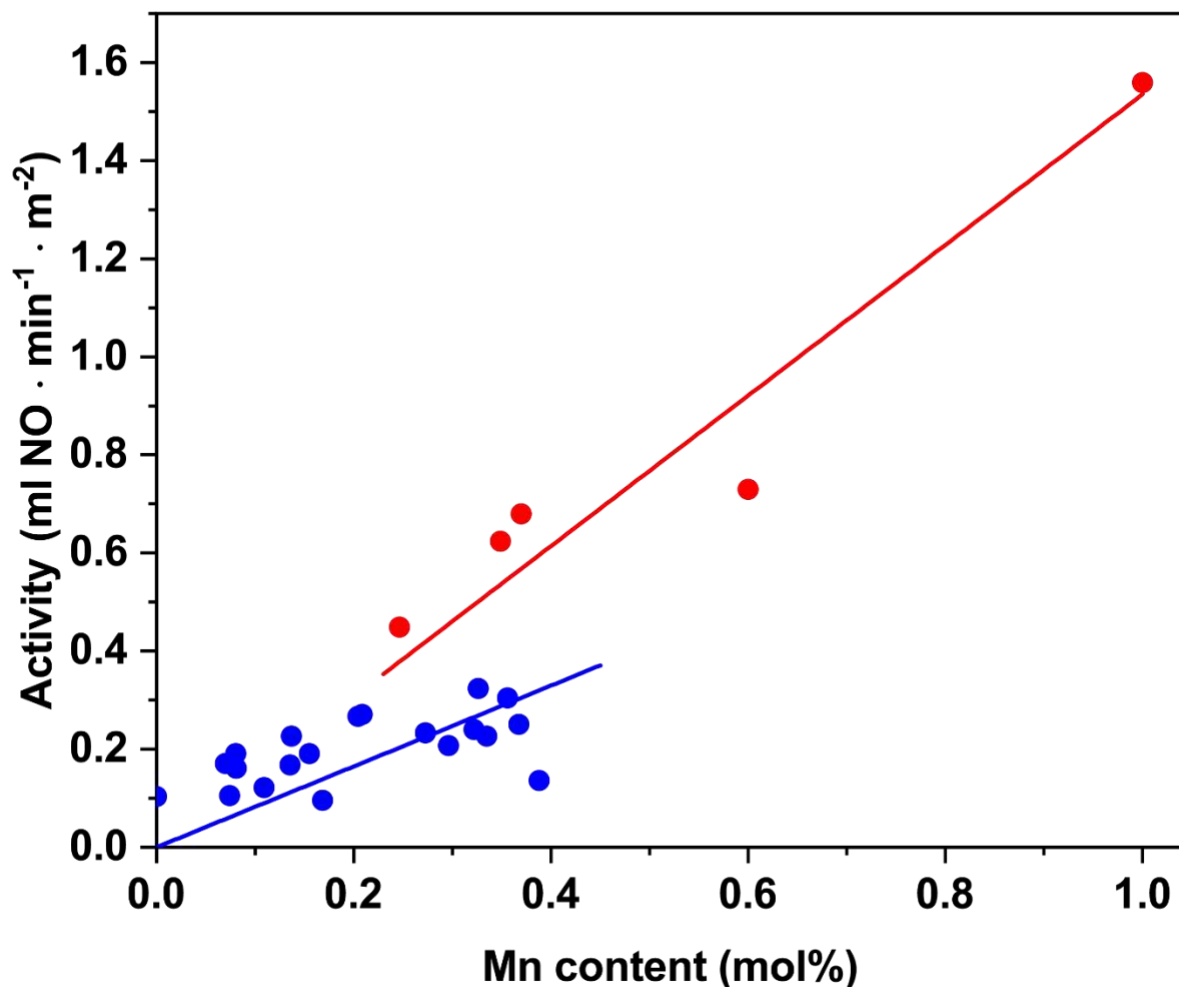
Fig. 6. Surface-specific activities for the NO reduction at 150 °C plotted as a function of the Mn content on the catalysts. The blue dots correspond to the ternary Mn-Ce-Ti catalysts. The red dots are from the binary Mn-Ti and the individual Mn catalysts. Red and blue trendlines were added to guide the eyes.

To assess the implication of the different MnOx species on catalytic performance, the normalized activities with the distinct Mn surface species (Mn^{4+}, Mn^{3+}, Mn^{2+} and total Mn) were constructed in Supplementary Fig. 10. The plots show an increase in activity with the amount of Mn^{4+} and Mn^{3+} species, however there are no direct evidences that the Mn^{2+} species are promoting catalyst activity, in line with previous reports[52]. Hence, the increase in the Mn^{2+} content in the samples containing Ce could, to a certain extent, explain the lower specific activity of those samples. In addition, the substantial effect of Ce on the TPR profiles, shifting reduction peaks of Mn^{4+} and Mn^{3+} to higher temperatures, indicates that other interactions of Mn^{4+} and Mn^{3+} with Ce species can be responsible for the lower specific activity.

235 We further investigated the nature of the oxygen species in the solid catalyst, which has been

236 suggested to have a significant impact on SCR activity, more specifically on the oxidation reactions[53,

237 54]. The reactivity of oxygen species on the catalyst was investigated by monitoring the formation of

238 N_2O during NH_3-TPD experiments. In these experiments, N_2O is formed in the range of 140 to 440 ^oC

239 via the oxidation of ammonia with active oxygen species on the catalyst surface. The plots in

240 supplementary Fig. 11. shows that NO activities at 150 ^oC are correlated to the amount of evolved N_2O

241 during NH_3-TPD experiments. pointing to the direct key role of the active oxygen in overall reaction

242 mechanism at low temperature. Since the NO activity is related to Mn content, we can infer that those

243 active oxygen species are related to Mn species.

244 The effect of Ce on the Mn activity has been previously reported in the literature with inconsistent

245 findings. For example, Liu et al. proposed a positive effect of Ce and Ti in activity by a dual redox cycle

246 consisting of $Mn^{4+} + Ce^{3+} \leftrightarrow Mn^{3+} + Ce^{4+}$ and $Mn^{4+} + Ti^{3+} \leftrightarrow Mn^{3+} + Ti^{4+}$ cycles[31]. A different

247 explanation of the beneficial effect of Ce was proposed by Yang et al., based on a mechanistic study

248 using *in-situ* FTIR spectroscopy. The authors suggested that MnOx species show a faster rate for the

249 conversion of NO to nitrate or nitrite, whereas CeO_2 mainly provides adsorption sites resulting in

250 nitrites species[29]. In line with our results, Wu et al. also observed a negative effect of Ce in the activity

251 in ternary Mn-Ce-Ti compared to binary Mn-Ti. However, these authors explained the negative effect

252 of Ce by a reduction in the Mn^{4+}/Mn^{3+} ratio [36]. In order to resolve the origin of these contradicting

253 findings, our results were contrasted with previously reported ones after surface-area normalization

254 of the activity data. These data are shown in Supplementary Table 8. The analysis shows that when

255 the activities are surface-area normalized, there is no positive effect of the addition of Ce on the

256 specific Mn activity, which validates our experimental results. Although this analysis is incomplete due

257 to our lack of knowledge on several parameters, such as Mn surface composition, oxidation states,

258 degree of interaction between the different oxide species, etc., there is no apparent trend pointing to

259 an increase in activity by Ce addition. Therefore, we propose that Ce is not improving the catalytic

260   properties of Mn species at low reaction temperatures and that the only promotional effect is purely

261   structural due to an increase in catalyst surface area.

262   When looking at the catalytic performance at higher temperatures, the role of Ce is clear.

263   Supplementary Fig. 12 shows NOx conversion of selected samples with increasing the amount of Ce.

264   The activity data of all catalyst samples can be found in supplementary table S7. The binary MnTi

265   catalysts has the highest activity at low temperatures, but the catalytic performance drastically drops

266   at temperatures higher than 250 °C due to the unselective oxidation of NH_3 to NOx. The addition of

267   Ce drops the conversion at low temperatures, but promotes NO_x conversion at temperatures higher

268   than 250 °C, widening the operational temperature window of the catalyst materials. Understanding

269   this effect lies beyond the scope of our investigations as other parameters, such as close proximity of

270   the redox and acidic functions, may govern the reaction at high temperatures[56].

271

272   **Role of Mn and Ce on N_2O selectivity at low temperature**

273   Finally, the N_2O formation at low temperature was investigated on all the samples. Possible effects of

274   conversion on N_2O selectivity were ruled out by inspecting the N_2O selectivity plot as function of

275   conversion in Supplementary Fig. 13. In general, the N_2O formed over MnO_x and binary Mn-Ti catalysts

276   is significantly higher than in the Mn-Ce-Ti ternary systems. For a deeper analysis of the selectivity

277   results, the surface-specific formation of N_2O of selected samples was plotted in Fig. 7 as function of

278   the Mn surface density calculated from the XPS measurements. The results clearly show an

279   exponential increase of the N_2O formation at 150 °C with the Mn surface density, indicating that N_2O

280   formation obeys a higher-than-one-order dependence in Mn. Our characterization and NO_x activity

281   measurements pointed to an interaction of Ce with Mn, leading to a decrease in the Mn activity. This

282   can definitely play a role in the lower N_2O activity but does not fully describe the Mn order

283   dependence. A plausible explanation of this behavior is that more than one Mn active species in close

284   proximity must participate in the kinetic formation of N_2O. According to literature, two main reaction

285 mechanisms explain the formation of N_2O at low temperature[57]: one base on a Langmuir-Hinshelwood

286 mechanism where NO is oxidized to NO_3^- species that react with NH_4^+ to give N_2O, and the other is an

287 Eley-Rideal mechanism resulting from the oxidative dehydrogenation of NH_3 to NH species that react

288 with NO to yield N_2O. A mechanistic study on the formation of N_2O is beyond the goal of this work,

289 but both proposed mechanisms are based on multistep oxidation of NO and/or NH_3. Therefore, we

290 postulate that the formation of N_2O requires the participation of at least two Mn active sites and that

291 is promoted by neighboring Mn active sites. The homogeneous composition of the ternary Mn-Ce-Ti

292 dilutes the Mn species on the catalyst surface and inhibits subsequent oxidation steps by breaking up

293 the MnOx ensembles. This mechanism is schematically depicted in Fig. 8. Besides the dilution effect,

294 the addition of Ce could also decrease the activity of surface oxygen observed by a suppressed N_2O

295 formation in the NH_3-TPD.
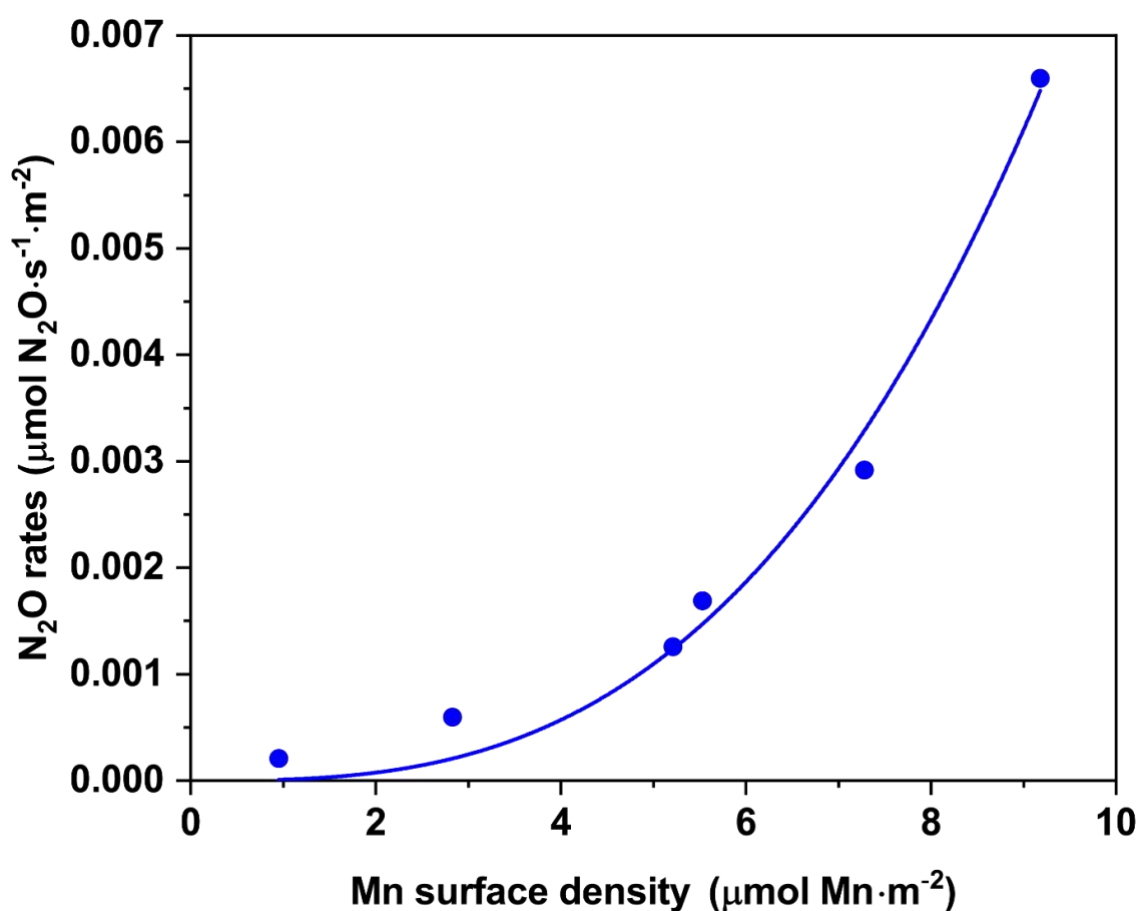
296

297 **Fig. 7**. surface-specific N_2O rates at 150 ^{o}C as a function of the Mn surface density. Samples from lower to higher
298 Mn surface density: $Mn_{0.08}Ce_{0.55}Ti_{0.37}$, $Mn_{0.14}Ce_{0.13}Ti_{0.74}$, $Mn_{0.21}Ce_{0.25}Ti_{0.54}$, $Mn_{0.30}Ce_{0.19}Ti_{0.51}$, $Mn_{0.36}Ce_{0.04}Ti_{0.60}$,
299 $Mn_{0.35}Ce_{0.00}Ti_{0.65}$. The blue line is a guide to the eye suggesting an exponential-type trend.

300   To rule out the effect of the amount of ammonia adsorbed on the catalysts on N_2O selectivity , NH_3-

301   TPD measurements were performed and the total number of acid sites, obtained from the total

302   amount of ammonia adsorbed, was plotted as a function of Ce content (Supplementary Fig. 13). The

303   total acidity of all the samples was also plotted in the ternary diagram in Supplementary Fig. 14. The

304   total acidity is around 1.1 $\mu mol/m^2$ up to 20% Ce and then monotonically increases up to around 2.5

305     $\mu mol/m^2$. Owing to the fact that the inhibiting of N_2O formation is observed in catalysts with Ce

306   content below 20%, we can exclude the role of the number of acid sites on the N_2O formation.

Manganese Oxide   Titanium Oxide   Cerium Oxide
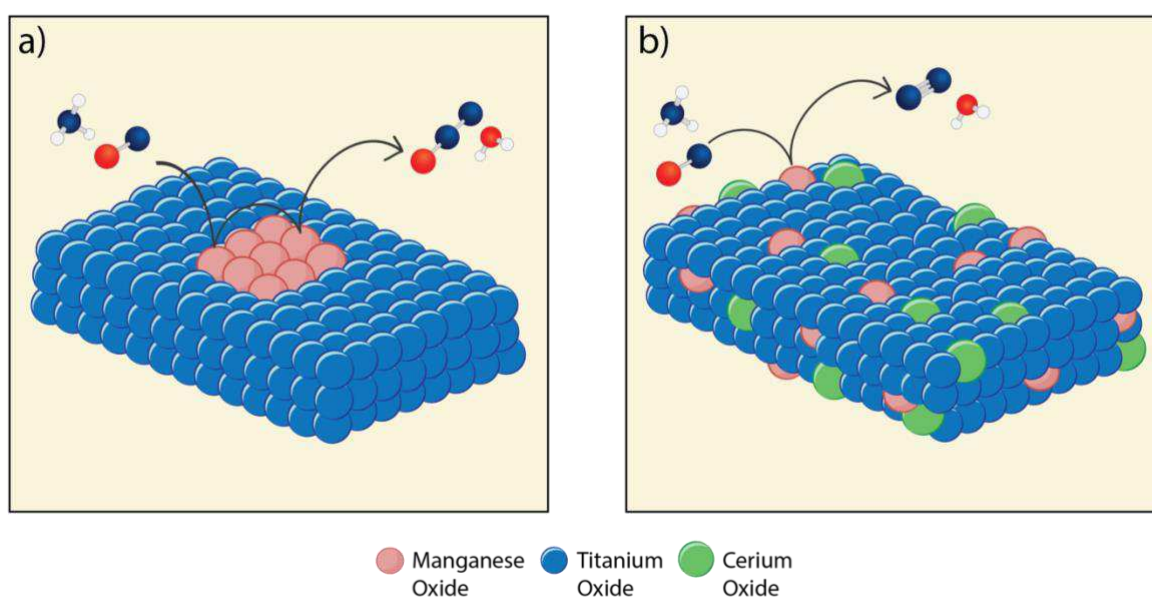
307
308   **Fig. 8**. A schematic representation of the reaction mechanism in a) a MnTi binary catalyst where the close
309   proximity of MnOx species promote the formation of N_2O and b) a MnCeTi ternary catalyst in which the well-
310   mixed amorphous structure promotes the spacing of MnOx species and therefore reduces the formation of N_2O.

311

312   Concluding, our research results add new insight into our understanding of Mn catalysts for low-

313   temperature NH_3-SCR applications and provides a direction towards settling the ongoing debate over

314   the effect of Ce on the Mn active species. We postulate that the activity of the Mn active sites is not

315   positively affected by Ce species in intimate contact. In fact, our results suggest that Ce is decreasing

316   the average oxidation state and activity of Mn active species and is just a structural promotor,

317   increasing catalyst surface area. On the other hand, addition of Ce is increasing N_2 selectivity as it

318 suppresses second step oxidation and thus N_2O formation by a dilution effect on the MnOx active

319 sites. The latter still makes Ce an attractive additive for Mn-Ti systems.

320

321 **Methods**

322 **Catalyst preparation.** Titanium(IV) sulfate solution ($Ti(SO_4)_2$, Pfaltz & Bauer., 30 % in H_2SO_4), cerium(III)

323 nitrate hexahydrate ($Ce(NO_3)_3 \cdot 6H_2O$, Sigma-Aldrich, 99.999% trace metals basis), manganese(II)

324 nitrate hydrate ($Mn(NO_3)_2 \cdot xH_2O$, Sigma-Aldrich, 99.999% trace metals basis), ammonium hydroxide

325 (NH_4OH, Alfa Aesar, ACS grade, 28.0-30.0%) were used as received, without further purification.

326 A series of individual, binary and ternary materials with different molar concentrations were prepared

327 by a controlled co-precipitation method as described in the Supplementary information and

328 Supplementary Fig. 1. Our method is a novel and highly efficient approach, where the aim is to

329 precipitate all metals at the same pH level to obtain a homogeneously well-mixed metal oxide system.

330 This is done by dual dosing of NH_3 and salt solution at a constant predetermined volumetric ratio. In

331 most literature, the salt solution is added dropwise to an NH_3 solution, but this gives a pH change over

332 time (from high to final low pH) and could lead to a suboptimal co-precipitation of the elements. First

333 manganese nitrate hydrate ($Mn(NO_3)_2 \cdot xH_2O$), and cerium nitrate ($Ce(NO_3)_3.6H_2O$) were dissolved in

334 deionized water and stirred for 10 minutes. Then, a 30% titanium sulfate solution [$Ti(SO_4)_2$) in H_2SO_4]

335 was added to the salt solution. These solutions were mixed under magnetic stirring at a constant

336 speed (400 rpm) for 30 minutes, leading to a perfectly mixed metal salt solution. The mixed metal salt

337 solution (loaded in a syringe pump) was injected simultaneously along with 14.7 M solution of

338 ammonium hydroxide with a Gilson pump (NH_4OH, Sigma-Aldrich, 97%) to a recipient containing 20

339 ml of mother solution that is already at the target pH of 10.5. During this simultaneous injection of

340 the metal precursor and base, the resulting suspension was continuously stirred. This procedure

341 allows to operate at a constant pH of around 10.5 by adding the same amount of hydroxide consumed

342 during the catalyst precipitation reaction. The metal oxides will precipitate at the same time,

343   rendering a very high level of homogeneity. Then, the precipitated solution was stirred for 30 min at

344   400 rpm. The sample was centrifuged at 7000 rpm and washed several times with milli-Q water until

345   the conductivity of the supernatant reached to 50 μs.cm^{-1}. Then the samples were dried overnight at

346   100 °C, followed by calcination at 500 °C for 6 h. The list of samples and compositions is shown in

347   Supplementary Table 1.

348   **Catalyst characterization.** X-ray diffraction patterns were obtained using a Bruker D8 Advanced A25

349   diffractometer in Bragg-Brentano geometry with Cu K$_{\alpha, \beta}$ radiation source operated at 40 kV and 40

350   mA. β radiation is filtered out with a Ni plate. The diffractograms were measured with step size of

351   0.05° in the 2θ range of 10–80°. Nitrogen adsorption and desorption isotherms of the samples were

352   measured at 77 K using Micromeritics ASAP-2420 surface area and porosity analyzer instrument.

353   Samples were previously evacuated at 300 °C for 3 hours. Specific surface areas and pore size

354   distribution were calculated according to multi-point Brunauer–Emmett–Teller (BET) and Barret–

355   Joyner–Halenda (BJH) method, respectively. From the adsorption data, total pore volumes were

356   estimated at P/P$_0$ = 0.99. The elemental compositions (Mn, Ce, Ti) of the samples were determined by

357   an inductively coupled plasma spectrometer (Model 8900, Agilent Technologies). The samples were

358   dissolved in HF and HCl. High-resolution Kratos Axis Ultra X-ray photoelectron spectroscopy equipped

359   with a monochromatic Al Kα source was used to determine the surface composition and chemical

360   states of the samples. All analyses were monitored using the C 1s signal for adventitious carbon (284.8

361   eV). The chemical states of manganese in the catalysts were determined by peak modeling in CasaXPS

362   software. To model the Mn 2p$_{3/2}$ peaks of the catalysts, pure MnO, Mn$_2$O$_3$ and MnO$_2$ samples were

363   used as reference. Manganese(IV) oxide (99.997% - metals basis) was acquired from Alfa Aesar (Fisher

364   US), manganese(III) oxide (99.9% - trace metals basis) was acquired from Sigma Aldrich, and

365   manganese(II) oxide (99.99% - trace metal basis) was acquired from Acros Organics (VWR). The fitting

366   parameters data (FWHM and Peak positions) obtained from the peak modelling of the standard

367   samples were used for the calculation of the chemical state of manganese in our catalysts. H$_2$-TPR

368   experiments were performed in Autochem 2950 instrument equipped with a thermal conductivity

369   detector. All catalysts (100 mg) were pretreated in a U-shaped quartz tubular micro-reactor in a flow

370   of Ar at 250 $^{\circ}$C for 2 h to yield a clean surface and then cooled down to 40 $^{\circ}$C. Then, the temperature

371   was raised from 40 to 1000 °C at a rate of 10 K/min under a flow of 10 vol. % H_2 (90 vol. % Ar). The

372   acidity of samples was determined by temperature-programmed desorption of ammonia (NH_3-TPD).

373   NH_3-TPD of samples was performed in a fixed bed quartz tube reactor. Prior to the measurement, the

374   samples were first pretreated at 500 °C under N_2 flow. The reactor was cool down at 100 °C and

375   samples were saturated with 1050 ppm NH_3 for 30 min. The samples were flush with N_2 for 30 min at

376   room temperature, and then the temperature was increased to 500 °C at a rate of 10 K/min. The outlet

377   gas composition (NH_3, NO, NO_2, N_2O) was monitored by using a MultiGas™ 2030 FTIR Continuous Gas

378   Analyzer. High-resolution transmission electron microscopy (HRTEM) micrographs obtained from a

379   Titan 60–300 TEM (FEI Co, Netherlands) equipped with an electron emission gun operating at 200 kV.

380   The annular Dark-Field scanning transmission electron microscopy (ADF-STEM) in conjunction with

381   electron energy loss spectroscopy (EELS) study was carried out with a Cs-Probe Corrected Titan

382   microscope (Thermo-Fisher Scientific) which was also equipped with a GIF Quantum of model 966

383   from Gatan Inc. (Pleasanton, CA). STEM-EELS analysis was performed by operating the microscope at

384   the accelerating voltage of 300 kV, using a convergence angle α of 17 mrad and a collection angle β

385   of 38 mrad. Spectrum-imaging dataset includes the simultaneous acquisition of zero-loss and core-

386   loss spectra (DualEELS) using a dispersion of 0.5 eV/channel and were recorded using a beam current

387   of 0.2 nA and a dwell time of 50 ms/pixel. The Ti $L_{2,3}$-edge, Mn $L_{2,3}$-edge, and Ce $M_{4,5}$-edge were

388   selected to build the chemical maps.

389   **Catalyst testing.** The catalytic activity measurements of the catalysts in the NH_3-SCR reaction were

390   carried out in a fixed bed quartz tube reactor loaded with 0.5 ml of sample (PID Eng&Tech). Before

391   loading, the catalysts were pressed into pellets, crushed and sieved to obtain a fraction between 500

392   and 710 μm. The total flow was maintained at 1000 ml/min, and the reaction condition corresponds

393   to GHSV of 120,000 hr^{-1}. The flow rate of gases was controlled using Bronkhorst mass flow controllers.

394   A Controlled Evaporation and Mixing system (CEM) from Bronkhorst was used for evaporation of the

395   required H_2O in the gas feed before entering the reactor. The inlet gas stream contained 450 ppm NO,

396   500 ppm NH_3, 5 % O_2, 5 % H_2O and N_2 balance. A MultiGas™ 2030 FTIR Continuous Gas Analyzer was

397   used to analyze the inlet and outlet gas compositions (NO, NO_2, NH_3, N_2O). The catalytic tests were

398   performed in the temperature range of 150 – 500 ˚C (with an interval of 50 ˚C) at ambient pressure.

399   The SCR activity (NO conversion) and N_2 selectivity are calculated as follows:

400
$$NO\ conversion\ (\%) = \frac{[NO]_{in} - [NO]_{out}}{[NO]_{out}} \times 100$$

401
$$N_2O\ selectivity\ (\%) = \frac{2[N_2O]_{out}}{[NO_x]_{in} + [NH_3]_{in} - [NO_x]_{out} - [NH_3]_{out}} \times 100$$

402   Where $[NH_3]_{in}$, $[NO_x]_{in}$, $[NH_3]_{out}$, $[NO_x]_{out}$, and $[N_2O]_{out}$ were the concentrations of NH_3 and

403   NO_x(including NO and NO_2) at the inlet and those at the outlet.

404

405   **Data Availability**

406   The data supporting the findings of this article are available in the paper and in the Supplementary

407   Information. Additional data are available from the corresponding author on reasonable request.

408

409

410   **Reference**

411   1.   Sorrels, J. L., Selective Catalytic Reduction. U.S. Enviromental Protection Agency.
412   https://www.epa.gov/economic-and-cost-analysis-air-pollution-regulations/chapter-2-selective-
413   catalytic-reduction. 2019.
414   2.   Zhang, R.; Liu, N.; Lei, Z.; Chen, B., Selective Transformation of Various Nitrogen-Containing
415   Exhaust Gases toward N2 over Zeolite Catalysts. *Chemical Reviews* **2016,** *116* (6), 3658-3721.
416   3.   Han, L.; Cai, S.; Gao, M.; Hasegawa, J. Y.; Wang, P.; Zhang, J.; Shi, L.; Zhang, D., Selective
417   Catalytic Reduction of NOx with NH3 by Using Novel Catalysts: State of the Art and Future Prospects.
418   *Chemical Reviews* **2019,** *119* (19), 10916-10976.
419   4.   Johnson, T. V., Diesel emission control in review. *SAE international journal of fuels and
420   lubricants* **2009,** *1* (1), 68-81.
421   5.   Bull, I. X., Wen-Mei; Burk, Patrick; Boorse, R. Samuel; Jaglowski, William M.; Koermer, Gerald
422   S.; Moini, Ahmad; Patchett, Joseph A.; Dettling, Joseph C.; Caudle, Matthew T. Copper CHA zeolite
423   catalyst. US7601662B2, 2009.
424   6.   Fickel, D. W.; Lobo, R. F., Copper coordination in Cu-SSZ-13 and Cu-SSZ-16 investigated by
425   variable-temperature XRD. *The Journal of Physical Chemistry C* **2010,** *114* (3), 1633-1640.
426   7.   Girard, J.; Cavataio, G.; Snow, R.; Lambert, C., Combined Fe-Cu SCR systems with optimized
427   ammonia to NOx ratio for diesel NOx control. *SAE International Journal of Fuels and Lubricants* **2009,**
428   *1* (1), 603-610.
429   8.   Kwak, J. H.; Tonkyn, R. G.; Kim, D. H.; Szanyi, J.; Peden, C. H., Excellent activity and
430   selectivity of Cu-SSZ-13 in the selective catalytic reduction of NOx with NH3. *Journal of Catalysis*
431   **2010,** *275* (2), 187-190.
432   9.   Chen, J.; Yang, R., Role of WO3 in mixed V2O5-WO3/TiO2catalysts for selective catalytic
433   reduction of nitric oxide with ammonia. *Applied Catalysis A: General* **1992,** *80* (1), 135-148.
434   10.   Xu, T.; Wu, X.; Gao, Y.; Lin, Q.; Hu, J.; Weng, D., Comparative study on sulfur poisoning of
435   V2O5-Sb2O3/TiO2 and V2O5-WO3/TiO2 monolithic catalysts for low-temperature NH3-SCR.
436   *Catalysis Communications* **2017,** *93*, 33-36.
437   11.   Tian, X.; Xiao, Y.; Zhou, P.; Zhang, W.; Luo, X., Investigation on performance of V2O5–
438   WO3–TiO2–cordierite catalyst modified with Cu, Mn and Ce for urea-SCR of NO. *Materials Research
439   Innovations* **2014,** *18* (sup2), S2-202-S2-206.
440   12.   Lian, Z.; Li, Y.; Shan, W.; He, H., Recent Progress on Improving Low-Temperature Activity of
441   Vanadia-Based Catalysts for the Selective Catalytic Reduction of NOx with Ammonia. *Catalysts* **2020,**
442   *10* (12), 1421.
443   13.   Narkhede, V.; Kumar, D.; Cursetji, R. M.; Sidiquie, T. A., Low Temperature Selective Catalytic
444   Reduction of NOx over Vanadium-Based Catalysts. SAE International: 2015.
445   14.   Weiss, M.; Paffumi, E.; Clairotte, M.; Drossinos, Y.; Vlachos, T.; Bonnel, P.; Giechaskiel, B.,
446   Including cold-start emissions in the Real-Driving Emissions (RDE) test procedure effects. *Including
447   Cold-Start Emissions in the Real-Driving Emissions (RDE) Test Procedure* **2017**.
448   15.   Chatterjee, S.; Naseri, M.; Li, J., Heavy Duty Diesel Engine Emission Control to Meet BS VI
449   Regulations. SAE International: 2017.
450   16.   Singoredjo, L.; Korver, R.; Kapteijn, F.; Moulijn, J., Alumina supported manganese oxides for
451   the low-temperature selective catalytic reduction of nitric oxide with ammonia. *Applied Catalysis B:
452   Environmental* **1992,** *1* (4), 297-316.
453   17.   Jin, R.; Liu, Y.; Wang, Y.; Cen, W.; Wu, Z.; Wang, H.; Weng, X., The role of cerium in the
454   improved SO2 tolerance for NO reduction with NH3 over Mn-Ce/TiO2 catalyst at low temperature.
455   *Applied Catalysis B: Environmental* **2014,** *148*, 582-588.
456   18.   Pappas, D. K.; Boningari, T.; Boolchand, P.; Smirniotis, P. G., Novel manganese oxide
457   confined interweaved titania nanotubes for the low-temperature Selective Catalytic Reduction (SCR)
458   of NOx by NH3. *Journal of Catalysis* **2016,** *334*, 1-13.

459   19.   Thirupathi, B.; Smirniotis, P. G., Nickel-doped Mn/TiO2 as an efficient catalyst for the low-
460   temperature SCR of NO with NH3: Catalytic evaluation and characterizations. *Journal of Catalysis*
461   **2012,** *288*, 74-83.
462   20.   Xiong, Y.; Tang, C.; Yao, X.; Zhang, L.; Li, L.; Wang, X.; Deng, Y.; Gao, F.; Dong, L., Effect of
463   metal ions doping (M= Ti4+, Sn4+) on the catalytic performance of MnOx/CeO2 catalyst for low
464   temperature selective catalytic reduction of NO with NH3. *Applied Catalysis A: General* **2015,** *495*,
465   206-216.
466   21.   Tang, X.; Hao, J.; Xu, W.; Li, J., Low temperature selective catalytic reduction of NOx with
467   NH3 over amorphous MnOx catalysts prepared by three methods. *Catalysis Communications* **2007,** *8*
468   (3), 329-334.
469   22.   Kang, M.; Yeon, T. H.; Park, E. D.; Yie, J. E.; Kim, J. M., Novel MnOxCatalysts for NO
470   Reduction at Low Temperature with Ammonia. *Catalysis Letters* **2006,** *106* (1), 77-80.
471   23.   Kang, M.; Park, E. D.; Kim, J. M.; Yie, J. E., Manganese oxide catalysts for NOx reduction with
472   NH3 at low temperatures. *Applied Catalysis A: General* **2007,** *327* (2), 261-269.
473   24.   Smirniotis, P. G.; Sreekanth, P. M.; Pena, D. A.; Jenkins, R. G., Manganese oxide catalysts
474   supported on TiO2, Al2O3, and SiO2: A comparison for low-temperature SCR of NO with NH3.
475   *Industrial & engineering chemistry research* **2006,** *45* (19), 6436-6443.
476   25.   Ettireddy, P. R.; Ettireddy, N.; Mamedov, S.; Boolchand, P.; Smirniotis, P. G., Surface
477   characterization studies of TiO2 supported manganese oxide catalysts for low temperature SCR of
478   NO with NH3. *Applied Catalysis B: Environmental* **2007,** *76* (1), 123-134.
479   26.   Wan, Y.; Zhao, W.; Tang, Y.; Li, L.; Wang, H.; Cui, Y.; Gu, J.; Li, Y.; Shi, J., Ni-Mn bi-metal
480   oxide catalysts for the low temperature SCR removal of NO with NH3. *Applied Catalysis B:*
481   *Environmental* **2014,** *148-149*, 114-122.
482   27.   Chen, Z.; Wang, F.; Li, H.; Yang, Q.; Wang, L.; Li, X., Low-Temperature Selective Catalytic
483   Reduction of NOx with NH3 over Fe–Mn Mixed-Oxide Catalysts Containing Fe3Mn3O8 Phase.
484   *Industrial & Engineering Chemistry Research* **2012,** *51* (1), 202-212.
485   28.   Liu, Z.; Liu, Y.; Li, Y.; Su, H.; Ma, L., WO3 promoted Mn–Zr mixed oxide catalyst for the
486   selective catalytic reduction of NOx with NH3. *Chemical Engineering Journal* **2016,** *283*, 1044-1050.
487   29.   Qi, G.; Yang, R. T.; Chang, R., MnOx-CeO2 mixed oxides prepared by co-precipitation for
488   selective catalytic reduction of NO with NH3 at low temperatures. *Applied Catalysis B: Environmental*
489   **2004,** *51* (2), 93-106.
490   30.   Machida, M.; Uto, M.; Kurogi, D.; Kijima, T., MnOx–CeO2 Binary Oxides for Catalytic NOx
491   Sorption at Low Temperatures. Sorptive Removal of NOx. *Chemistry of Materials* **2000,** *12* (10),
492   3158-3164.
493   31.   Liu, Z.; Zhu, J.; Li, J.; Ma, L.; Woo, S. I., Novel Mn–Ce–Ti Mixed-Oxide Catalyst for the
494   Selective Catalytic Reduction of NOx with NH3. *ACS Applied Materials & Interfaces* **2014,** *6* (16),
495   14500-14508.
496   32.   Eigenmann, F.; Maciejewski, M.; Baiker, A., Selective reduction of NO by NH3 over
497   manganese–cerium mixed oxides: Relation between adsorption, redox and catalytic behavior.
498   *Applied Catalysis B: Environmental* **2006,** *62* (3), 311-318.
499   33.   Wu, Z.; Jin, R.; Liu, Y.; Wang, H., Ceria modified MnOx/TiO2 as a superior catalyst for NO
500   reduction with NH3 at low-temperature. *Catalysis Communications* **2008,** *9* (13), 2217-2220.
501   34.   Xie, S.; Li, L.; Jin, L.; Wu, Y.; Liu, H.; Qin, Q.; Wei, X.; Liu, J.; Dong, L.; Li, B., Low
502   temperature high activity of M (M= Ce, Fe, Co, Ni) doped M-Mn/TiO2 catalysts for NH3-SCR and in
503   situ DRIFTS for investigating the reaction mechanism. *Applied Surface Science* **2020**, 146014.
504   35.   Li, L.; Wu, Y.; Hou, X.; Chu, B.; Nan, B.; Qin, Q.; Fan, M.; Sun, C.; Li, B.; Dong, L.; Dong, L.,
505   Investigation of Two-Phase Intergrowth and Coexistence in Mn–Ce–Ti–O Catalysts for the Selective
506   Catalytic Reduction of NO with NH3: Structure–Activity Relationship and Reaction Mechanism.
507   *Industrial & Engineering Chemistry Research* **2019,** *58* (2), 849-862.

508   36.   Wu, X.; Si, Z.; Li, G.; Weng, D.; Ma, Z., Effects of cerium and vanadium on the activity and
509   selectivity of MnOx-TiO2 catalyst for low-temperature NH3-SCR. *Journal of Rare Earths* **2011,** *29* (1),
510   64-68.
511   37.   Niu, Y.; Shang, T.; Hui, S.; Zhang, X.; Lei, Y.; Lv, Y.; Wang, S., Synergistic removal of NO and
512   N2O in low-temperature SCR process with MnOx/Ti based catalyst doped with Ce and V. *Fuel* **2016,**
513   *185*, 316-322.
514   38.   Wang, Q.; Zhou, J.; Zhang, J.; Zhu, H.; Feng, Y.; Jin, J., Effect of ceria doping on catalytic
515   activity and SO2 resistance of MnOx /TiO2 catalysts for selective catalytic reduction of NO with NH3
516   at low temperature. *Aerosol and Air Quality Research* **2020**.
517   39.   Nalbandian, L.; Delimitis, A.; Zaspalis, V.; Deliyanni, E.; Bakoyannakis, D.; Peleka, E.,
518   Hydrothermally prepared nanocrystalline Mn–Zn ferrites: synthesis and characterization.
519   *Microporous and Mesoporous Materials* **2008,** *114* (1-3), 465-473.
520   40.   Xu, W.; Yu, Y.; Zhang, C.; He, H., Selective catalytic reduction of NO by NH3 over a Ce/TiO2
521   catalyst. *Catalysis Communications* **2008,** *9* (6), 1453-1457.
522   41.   Qi, K.; Xie, J.; Zhang, Z.; Fang, D.; Han, D.; Liu, X.; Gong, P.; Li, F.; He, F., Facile large-scale
523   synthesis of CeMn composites by redox-precipitation and its superior low-temperature performance
524   for NO removal. *Powder Technology* **2018,** *338*, 774-782.
525   42.   Lee, S. M.; Park, K. H.; Hong, S. C., MnOx/CeO2–TiO2 mixed oxide catalysts for the selective
526   catalytic reduction of NO with NH3 at low temperature. *Chemical Engineering Journal* **2012,** *195-
527   196*, 323-331.
528   43.   Arena, F.; Torre, T.; Raimondo, C.; Parmaliana, A., Structure and redox properties of bulk
529   and supported manganese oxide catalysts. *Physical Chemistry Chemical Physics* **2001,** *3* (10), 1911-
530   1917.
531   44.   Wu, X.; Liang, Q.; Weng, D.; Fan, J.; Ran, R., Synthesis of CeO2–MnOx mixed oxides and
532   catalytic performance under oxygen-rich condition. *Catalysis Today* **2007,** *126* (3), 430-435.
533   45.   Giordano, F.; Trovarelli, A.; de Leitenburg, C.; Giona, M., A Model for the Temperature-
534   Programmed Reduction of Low and High Surface Area Ceria. *Journal of Catalysis* **2000,** *193* (2), 273-
535   282.
536   46.   Watanabe, S.; Ma, X.; Song, C., Characterization of Structural and Surface Properties of
537   Nanocrystalline TiO2–CeO2 Mixed Oxides by XRD, XPS, TPR, and TPD. *The Journal of Physical
538   Chemistry C* **2009,** *113* (32), 14249-14257.
539   47.   Yao, H.; Yao, Y. Y., Ceria in automotive exhaust catalysts: I. Oxygen storage. *Journal of
540   catalysis* **1984,** *86* (2), 254-265.
541   48.   Chen, J.; Chen, X.; Yan, D.; Jiang, M.; Xu, W.; Yu, H.; Jia, H., A facile strategy of enhancing
542   interaction between cerium and manganese oxides for catalytic removal of gaseous organic
543   contaminants. *Applied Catalysis B: Environmental* **2019,** *250*, 396-407.
544   49.   Biesinger, M. C.; Payne, B. P.; Grosvenor, A. P.; Lau, L. W. M.; Gerson, A. R.; Smart, R. S. C.,
545   Resolving surface chemical states in XPS analysis of first row transition metals, oxides and
546   hydroxides: Cr, Mn, Fe, Co and Ni. *Applied Surface Science* **2011,** *257* (7), 2717-2730.
547   50.   Leng, X.; Zhang, Z.; Li, Y.; Zhang, T.; Ma, S.; Yuan, F.; Niu, X.; Zhu, Y., Excellent low
548   temperature NH3-SCR activity over MnaCe0.3TiOx (a = 0.1–0.3) oxides: Influence of Mn addition.
549   *Fuel Processing Technology* **2018,** *181*, 33-43.
550   51.   Andreoli, S.; Deorsola, F. A.; Pirone, R., MnOx-CeO2 catalysts synthesized by solution
551   combustion synthesis for the low-temperature NH3-SCR. *Catalysis Today* **2015,** *253*, 199-206.
552   52.   Liu, C.; Shi, J.-W.; Gao, C.; Niu, C., Manganese oxide-based catalysts for low-temperature
553   selective catalytic reduction of NOx with NH3: A review. *Applied Catalysis A: General* **2016,** *522*, 54-
554   69.
555   53.   Marbán, G.; Valdés-Solís, T.; Fuertes, A. B., Mechanism of low-temperature selective
556   catalytic reduction of NO with NH3 over carbon-supported Mn3O4: Role of surface NH3 species: SCR
557   mechanism. *Journal of Catalysis* **2004,** *226* (1), 138-155.

558 54. Kapteijn, F.; Singoredjo, L.; Andreini, A.; Moulijn, J., Activity and selectivity of pure
559 manganese oxides in the selective catalytic reduction of nitric oxide with ammonia. *Applied Catalysis*
560 *B: Environmental* **1994,** *3* (2-3), 173-189.
561 55. Boningari, T.; Ettireddy, P. R.; Somogyvari, A.; Liu, Y.; Vorontsov, A.; McDonald, C. A.;
562 Smirniotis, P. G., Influence of elevated surface texture hydrated titania on Ce-doped Mn/TiO2
563 catalysts for the low-temperature SCR of NOx under oxygen-rich conditions. *Journal of Catalysis*
564 **2015,** *325*, 145-155.
565 56. Qu, W.; Liu, X.; Chen, J.; Dong, Y.; Tang, X.; Chen, Y., Single-atom catalysts reveal the
566 dinuclear characteristic of active sites in NO selective reduction with NH3. *Nature Communications*
567 **2020,** *11* (1), 1532.
568 57. Yang, S.; Xiong, S.; Liao, Y.; Xiao, X.; Qi, F.; Peng, Y.; Fu, Y.; Shan, W.; Li, J., Mechanism of
569 N2O Formation during the Low-Temperature Selective Catalytic Reduction of NO with NH3 over Mn–
570 Fe Spinel. *Environmental Science & Technology* **2014,** *48* (17), 10354-10362.

571

Acknowledgements

578

Author contribution

580 L.E.G. and J.R.M. conceived, coordinated the research, designed the experiments and analyzed the
581 data. L.R.E and A.S. synthesized the catalyst materials and characterized them by TPD and BET. L.R.E.
582 and A.S. performed the catalytic activity measurements. S.O.C. performed and analyzed the electron
583 microscopy measurements. A.S. and M.N.H. performed and analyzed the XPS measurements. L.R.E.,
584 A.S. performed the XRD measurements and P.P.P. conducted the analysis. J.R.M. wrote the
585 manuscript with the assistance of L.E.G., A.S. and L.R.E. All authors discussed the results and
586 commented on the manuscript.

587

Competing interest

589 The authors declare no competing interest.

Supplementary Files

This is a list of supplementary files associated with this preprint. Click to download.

- UnravelingtheStructureandRoleofMnandCeforSelectiveCatalyticReductionofNOinApplicationRelevantCatalystsandConditionsSuppinfo.pdf